Journal of Applied Physics

Critical condition of electrohydrodynamic jetting from a polymer-solution droplet on a conductive wire

Cite as: J. Appl. Phys. **127**, 054303 (2020); https://doi.org/10.1063/1.5132313
Submitted: 16 October 2019 . Accepted: 21 January 2020 . Published Online: 04 February 2020

Xiang-Fa Wu, Zhengping Zhou, Oksana Zholobko, Jeremy J. Jenniges, Brandon Baatz, Mojtaba Ahmadi, and Jiahui Chen

Journal of Applied Physics ARTICLE scitation.org/journal/jap

Critical condition of electrohydrodynamic jetting from a polymer-solution droplet on a conductive wire

Cite as: J. Appl. Phys. **127**, 054303 (2020); doi: 10.1063/1.5132313
Submitted: 16 October 2019 · Accepted: 21 January 2020 ·
Published Online: 4 February 2020

Xiang-Fa Wu,[a] Zhengping Zhou, Oksana Zholobko, Jeremy J. Jenniges, Brandon Baatz, Mojtaba Ahmadi, and Jiahui Chen

AFFILIATIONS

Department of Mechanical Engineering, North Dakota State University, Fargo, North Dakota 58108, USA

[a]**Author to whom correspondence should be addressed:** Xiangfa.Wu@ndsu.edu

ABSTRACT

An experimental study was conducted to determine the threshold electrostatic field to initiate electrohydrodynamic jetting from a polymer solution droplet wetting on a conductive wire. The study is crucial to understand the roles of the material and process parameters in wire-based needleless electrospinning for controllable mass production of continuous nanofibers. Two types of polymer solutions, i.e., polyacrylonitrile/N,N-dimethylformamide (PAN/DMF) and aqueous polyethyloxide solution (PEO/H_2O), with the mass concentrations of 4%, 8%, 12%, and 16% for PAN and 1%, 2%, 4%, 6%, and 8% for PEO, respectively, were considered in the experiments. Taut thin copper wires with diameters of 0.254, 0.508, 1.016, and 1.524 mm (i.e., 0.01, 0.02, 0.04, and 0.06 in.) were utilized, respectively, as the positive electrodes. The effects of the polymer concentration and wire diameter on the threshold electrical voltage for jetting initiation and nanofiber diameter were examined. Given the droplet volume and spacing between the copper wire and fiber collector, experimental observations show that the threshold electrical voltage increases with increasing either polymer mass concentration or wire diameter. In addition, the effects of polymer mass concentration on the transient shear viscosity and surface tension of the PAN/DMF solutions were examined. It shows the positive correlation between the transient shear viscosity and polymer mass concentration, shear thinning of the polymer solution at a high shear rate, and nearly constant surface tension of the polymer solution in the range of the present PAN mass concentration. Furthermore, a simple electrostatic model is formulated to phenomenologically elucidate the experimental observations. The present study provides useful scaling laws for controllable scale-up nanofiber fabrication by means of a wire-based needleless electrospinning technique.

I. INTRODUCTION

Electrospinning is a low-cost, top-down nanofiber manufacturing technique based on the principle of electrohydrodynamic jetting from polymer solutions or melts.[1–6] Electrospinning has been extensively utilized for fabricating a variety of ultrathin continuous fibers of polymers and polymer-derived carbon, silicon, metals, metal oxides, ceramics, etc., in various sizes and morphologies for broad applications including nanocomposites, high-grade gas/liquid filtration, tissue scaffolding and drug delivery, sensing, and energy harvesting, conversion and storage, among others.[5,7–13] A conventional electrospinning setup consists of a spinneret (i.e., a capillary tube) connected to a polymer solution pump, a high-voltage direct current (DC) power supply, and a fiber collector as illustrated in Fig. 1(a). During an electrospinning process, a droplet is initiated to form a Taylor cone under the action of an induced electrostatic field [see Fig. 1(b)].[14,15] With increasing the electrical field, the droplet is deformed and elongated. Once the electrostatic force acting on the droplet overcomes the surface tension of the droplet, a thin jet is ejaculated, stretched, and thinned in the electrostatic field until it loses stability in terms of vigorous jet whipping.[16–19] After a variety of jet stabilities accompanying fast solvent evaporation,[20–22] the extremely thinned jet is collected as a nonwoven fiber mat on the fiber collector. The fiber productivity of a conventional single-spinneret-based electrospinning setup is rather low, around a few grams of nanofibers per day, which significantly limits the broad applications of electrospun nanofibers if the bottleneck of continuous, scalable nanofabrication is not resolved.

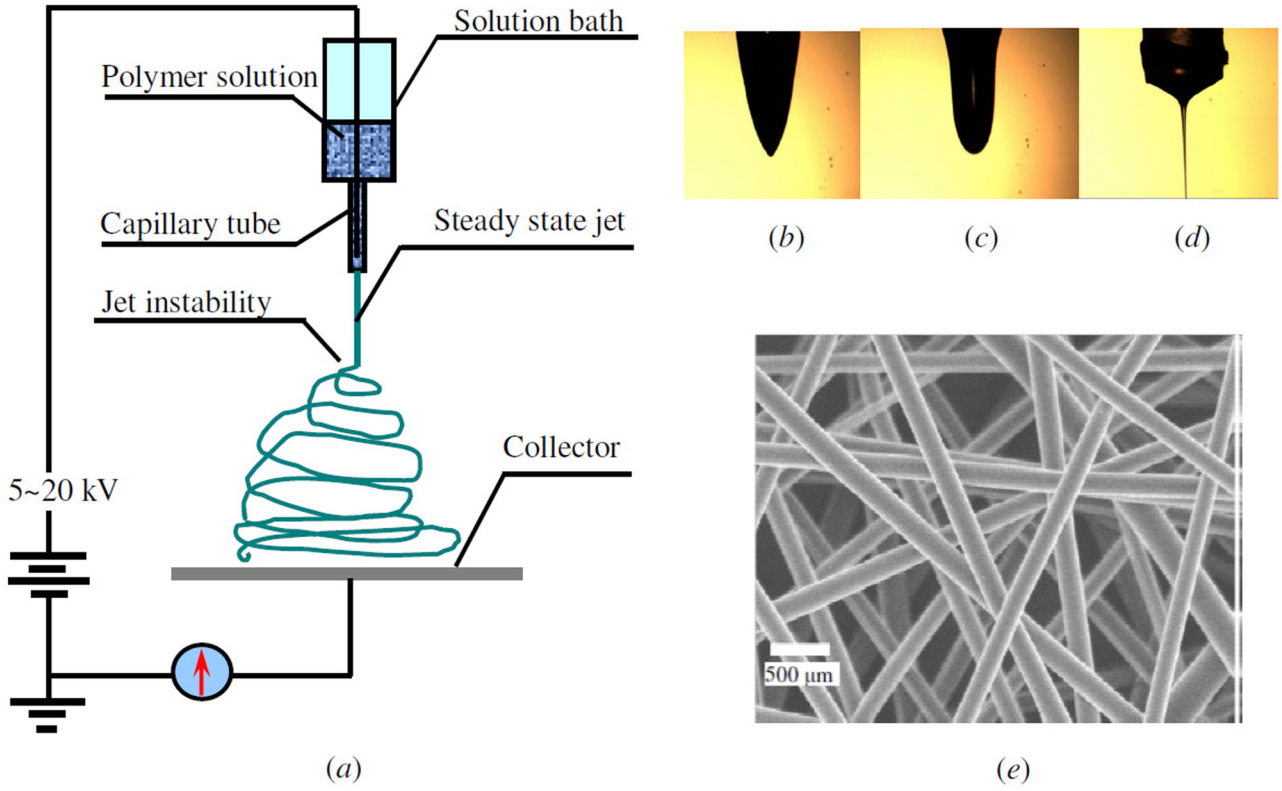

FIG. 1. Needle-based electrospinning process for continuous nanofiber fabrication: (a) schematic electrospinning setup, (b) Taylor cone (a deformed droplet in a biased DC electrostatic field), (c) an electrostatically stretched droplet, (d) a thin jet ejaculated in a stable electrospinning process, and (e) SEM micrograph of nonwoven electrospun polyacrylonitrile (PAN) nanofibers.

In the past two decades, significant efforts have been dedicated to overcoming the technical barriers of the conventional electrospinning technique for low-cost, mass fiber production, such as adoption of multiple spinnerets (e.g., eSpinner^{TM}), free-surface (needleless) electrospinning,[23–26] electrohydrodynamic jetting from porous surfaces,[27] twisted and dual wire-based electrospinning,[28,29] etc. Among these, with the birth of needleless electrospinning machine Nanospider^{TM} (Elmarco Inc., Czech), free-surface electrospinning has been demonstrated as a successful technique for continuous scalable nanofiber fabrication. During a needleless electrospinning process, Nanospider^{TM} is able to continuously maintain a thin layer of polymer solution with nearly constant thickness on a rotating cylindrical drum that is partially submerged into the polymer solution. When subjected to a biased external DC electrostatic field, the thin liquid layer of polymer solution destabilizes and triggers tens to hundreds of thin jets out of the free surface of the rotating drum depending upon the length and radius of the drum, which significantly enhances the nanofiber productivity. Furthermore, wire-based needleless electrospinning has also been adopted (e.g., Nanospider^{TM}), which can effectively avoid fast solvent evaporation from the polymer solution tank and better tune the fiber diameters. Its work mechanism is illustrated in Fig. 2 as follows. The polymer solution is continuously coated onto a thin conductive wire (e.g., a metal wire) by a solution cartridge installed with a cleaning wiper and the coated solution quickly destabilizes into symmetrical barrel-shaped droplets sitting on the wire [Fig. 2(a)].[30–35] When subjected to a biased electrostatic field via applying a high DC voltage between the conductive wire and the fiber collector (typically grounded), the droplets are deformed into nonsymmetrical clamshell-shaped droplets [Fig. 2(b)] and further stretched with increasing electrostatic field [Fig. 2(c)].[36–41] Finally, electrohydrodynamic jetting initiates from the extremely stretched droplets once the threshold electrostatic field is reached [Fig. 2(d)]. Figures 2(e) and 2(f) are the snapshots of multiple deformed droplets on a conductive wire in a biased electrostatic field and multiple-jet initiation therein. Figure 2(g) is a schematic setup for wire-based needleless electrospinning test, which consists of a tout straight metal wire as the positive electrode and a thin metal plate as the negative electrode and fiber collector (typically grounded). The main control parameters of a wire-based electrospinning process include material parameters [e.g., polymer type, polymer molecular weight, solvent type, polymer concentration, electric and dielectric properties of solvents (tunable with dissolvable salts or dielectric micelles), etc.] and process parameters [e.g., wire diameter, solution feeding rate (droplet size and spacing), electrostatic field, etc.]. A good electrospinning strategy for controllable mass production of continuous nanofibers is the combination

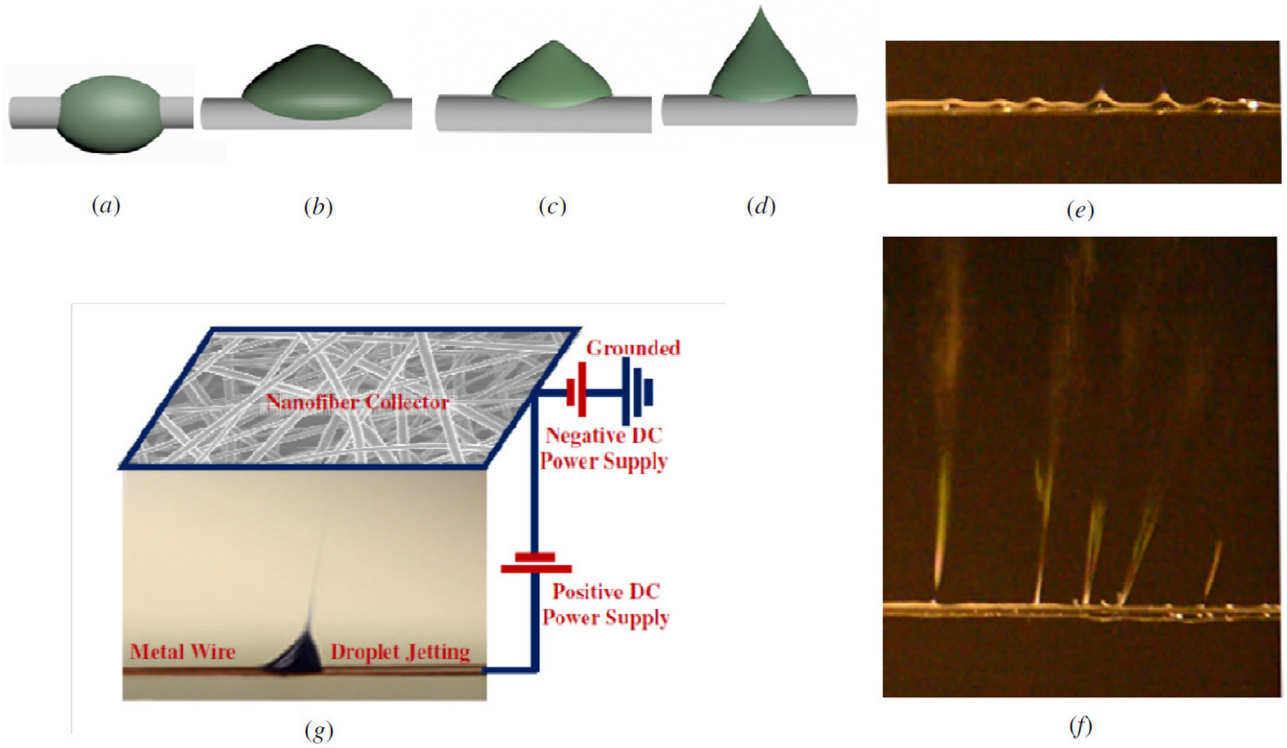

FIG. 2. Schematic and experimental observations of wire-based needleless electrospinning: (a) an schematic barrel-shaped droplet wetting on a taut conductive wire free of electrical field, (b) a droplet deformed into a clamshell-shaped droplet in a biased DC electrostatic field (in the vertical direction), (c) a stretched droplet in a large DC electrostatic field, (d) electrohydrodynamic jetting from a stretched droplet in a large DC electrostatic field, (e) a thin aqueous polyethyloxide (PEO) solution layer destabilizes into multiple droplets sitting on a tout copper wire in a biased electrostatic field, (f) multiple jets initiate from aqueous PEO solution droplets in a large biased electrostatic field, and (g) a schematic setup for wire-based needleless electrospinning.

of a set of material and process parameters that are typically optimized by trials and errors.

Though the concept of wire-based needleless electrospinning has been realized for continuous mass production of nanofibers, effects of these materials and process parameters on jetting initiation and nanofiber properties have not been systematically investigated yet. Therefore, in the present work, we conducted the experimental studies to explore effects of two key material and process parameters, namely, the polymer mass concentration and wire diameter, on the threshold electrostatic field for jetting initiation and the diameter of resulting nanofibers based on a lab-made setup as illustrated in Fig. 2(g). Two types of polymer solutions, i.e., polyacrylonitrile/N,N-dimethylformamide (PAN/DMF) and aqueous polyethyloxide solution (PEO/H_2O), with varying mass concentrations of 4%, 8%, 12%, and 16% for PAN and 1%, 2%, 4%, 6%, and 8% for PEO were utilized, respectively. Tout thin copper wires with diameters of 0.254, 0.508, 1.016, and 1.524 mm (i.e., 0.01, 0.02, 0.04, and 0.06 in.), respectively, were used as the positive electrode for the electrospinning test. A field-emission scanning electron microscope (FE-SEM, JEOL JSM-7600F, JEOL Ltd., Japan) was utilized for characterization of the morphology and diameter of the typical nanofibers collected in the present electrospinning test. Correlations of the threshold electrostatic field (voltage) and fiber diameter to the polymer solution and wire diameter were made. A simple electrostatic model was further proposed for a rational understanding of the experimental observations. Detailed discussions of the experimental results and conclusions of the present experimental study were made in consequence.

II. EXPERIMENTAL

PAN (Mw = 150 000 g/mol), PEO (Mw = 100 000 g/mol), and DMF (99%) were purchased from Sigma-Aldrich Co. (St Louis, MO). De-ionized (DI) water (H_2O) was obtained from a local chemical vendor. Four PAN/DMF solutions with PAN mass concentrations of 4%, 8%, 12%, and 16% were prepared, respectively, as follows. For each PAN concentration, the specified PAN powder was added to DMF under magnetic stirring. The mixture had been further stirred at 80 °C for 6 h to obtain a well-electrospinnable solution. Similarly, five aqueous PEO solutions with PEO mass concentrations of 1%, 2%, 4%, 6%, and 8% were prepared, respectively, via dissolving the specified PEO powder in DI H_2O. Each mixture had been further stirred at room temperature for 6 h.

Transient shear viscosity of the PAN/DMF solutions was characterized at room temperature using a TA ARG2 Rheometer (TA

Instruments, New Castle, DE). In the test, the shear rate was specified in the range from 1 up to 1000/s.

Surface tension of pure DMF and PAN/DMF solutions of varying PAN mass concentrations of 0.05%, 0.5%, 1%, 2%, 4%, 8%, and 12% was measured by means of the pendant drop method on a FTA 125 Contact Angle/Surface Energy Analyzer (First Ten Angstroms Inc., Portsmouth, VA). For each PAN/DMF solution, its surface tension was obtained via averaging the surface tension values extracted from seven independent measurements.

Wire-based needleless electrospinning test was conducted on a lab-made setup as illustrated in Fig. 2(g). The setup consists of a taut copper wire, with wire diameters of 0.254, 0.508, 1.016, and 1.524 mm (i.e., 0.01, 0.02, 0.04, and 0.06 in.), respectively, as the positive electrode connected to a positive high-voltage DC power supply and a rectangular steel plate (with the areal dimensions: 12×12 in.^{2} and thickness: 1/8 in.) connected to a negative high-voltage DC power supply with a fixed negative voltage of -2 kV to suppress nanofiber deposition onto surrounding utilities. Both the positive and negative DC power supplies were provided by the Gamma High Voltage Research Inc. (Ormond Beach, FL). Both the taut thin copper wire and plate were positioned horizontally, and the spacing from the copper wire to the plate was kept as 165.1 mm (6.5 in). The thin steel plate was also functioned as the nanofiber collector.

During an electrospinning test at room temperature with the relative humidity of ~45%, a droplet of either PAN/DMF or aqueous PEO solution with the volume of ~2.0 μl was placed symmetrically onto the taut copper wire at its midspan using an adjustable micropipette (Cole-Parmer, Vernon Hills, IL). The droplet quickly sat onto the wire to assume a stable symmetric barrel-shaped droplet,[30–35] and then the DC voltage between the copper wire and the steel plate was increased gradually until droplet jetting initiated. The corresponding DC voltage to initiate jetting was recorded as the threshold voltage. For each pair of polymer solution and wire diameter, at least 10 measurements were conducted and the average value of the corresponding threshold voltages was regarded as the threshold voltage for such a specific case.

In the case of PAN/DMF solutions, after each droplet jetting, typical PAN nanofibers were collected for characterization of their surface morphologies and diameters by using a FE-SEM (JEOL JSM-7600F, JEOL Ltd., Japan). Prior to SEM characterization, the PAN nanofiber samples were first sputter-coated with carbon to avoid possible charge accumulation onto the nanofibers during the SEM test. Image analysis was further performed to determine the statistical distribution of the diameters of typical nanofibers collected in the wire-based needleless electrospinning process for parameter correlations.

III. RESULTS AND DISCUSSION

A. Transient shear viscosity and surface tension

Figure 3 shows variations of the transient shear viscosity with varying shear rate for the PAN/DMF solutions with PAN mass concentrations of 4%, 8%, 12%, and 16%. Given a shear rate, the experimental transient shear viscosity increases with increasing PAN mass concentration. Meanwhile, given a PAN concentration, the transient shear viscosity is nearly constant at relatively low PAN concentrations (e.g., 4, 8, and 12 wt. %), while it decreases with

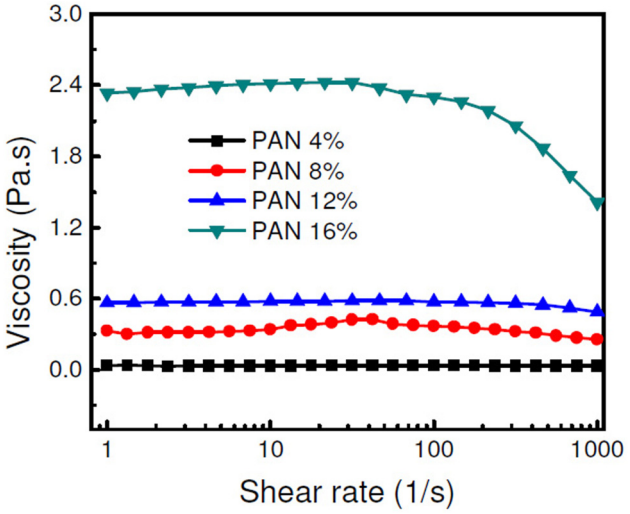

FIG. 3. Variation of the transient shear viscosity with varying shear rate for PAN/DMF solutions with four PAN mass concentrations of 4%, 8%, 12%, and 16%, respectively.

increasing shear rate at the high PAN concentration (i.e., 16 wt. %). In particular, when the shear rate is higher than 100 s^{-1}, the transient shear viscosity of the solution with PAN concentration of 16 wt. % decreases abruptly. This phenomenon resulted from the shear-thinning effect that typically appears in polymer solutions at a high shear rate.[42,43] In this case, the macromolecular chains of the polymer are highly stretched and aligned along the shearing direction and, therefore, have no sufficient time to relax. Even though the electrospinning jets were mainly under the action of extensional stretching, the measured transient shear viscosity can be used to justify the dynamic extensional viscosity based on the positive correlation between the two viscosities.[44] The rheological measurements also imply that highly aligned molecular chains in polymer nanofibers can be achieved via spinning high-concentration polymer solutions or melts at a high transient drawing rate.

Figure 4 shows the typical digital micrograph of a pendant droplet of the PAN/DMF solution captured by the FTA 125 Contact Angle/Surface Energy Analyzer (First Ten Angstroms, Inc., Portsmouth, VA). According to the pendant drop method, the surface tension γ of the PAN/DMF solution is determined as

$$\gamma = \frac{V\rho g}{\pi d}, \tag{1}$$

where V is the volume of the pendant droplet, ρ the mass density of the specific PAN/DMF solution under measurement, g the gravitational acceleration ($g = 9.81$ m/s^2), and d is the upper neck diameter of the pendant droplet. The surface tension of pure DMF and the PAN/DMF solution at each PAN mass concentration was obtained by averaging the surface tension values extracted from seven independent measurements. The reduced surface tensions of the PAN/DMF solutions with PAN mass concentrations of 0.05%, 0.5%, 1%, 2%, 4%,

FIG. 4. Typical digital micrograph of a pendant droplet captured by the FTA 125 Contact Angle/Surface Energy Analyzer (First Ten Angstroms, Inc., Portsmouth, VA).

8%, and 12%, respectively, are tabulated in Table I, which shows the surface tension nearly independent of the PAN mass concentration. It also needs to be mentioned that in the case of PAN mass concentration of 16%, the PAN/DMF solution was too viscous to form a stable pendant droplet. Thus, the pendant drop method is not workable for surface tension measurement in this case.

B. Critical condition for jetting initiation from polymer solution droplets

Figure 5 shows dependencies of the threshold DC electrical voltage to initiate droplet jetting upon the PAN mass concentration of the PAN/DMF solutions at four different wire diameters of 0.254, 0.508, 1.016, and 1.524 mm (i.e., 0.01, 0.02, 0.04, and 0.06 in.), respectively. Given a wire diameter and droplet volume (~2 μl), the threshold DC voltage increases with increasing PAN mass concentration. This observation can be understood such that in a polymer solution with a higher polymer concentration, the polymer chains tend to be more entangled, resulting in increasing solution viscosity. As a result, a higher electrostatic force is needed to trigger the droplet to initiate jetting because jetting initiation is an electrohydrodynamic process closely relevant to the transient behavior of the polymer solution, namely, a higher threshold voltage is needed at a given wire diameter and spacing between the wire and the fiber collector. Furthermore, at a fixed PAN mass concentration of the PAN/DMF solutions, the threshold voltage increases significantly with increasing wire diameter. Two dominate factors are responsible for such an observation. First, given the droplet volume of a PAN/DMF solution, a symmetrical barrel-shaped droplet sitting on a small-diameter wire more tends to destabilize into a nonsymmetrical clamshell-shaped droplet and even to be easily peeled off under a small biased force or electrostatic field.[36–41] Second, given the spacing and DC voltage between the wire electrode and the fiber collector, the wire with a smaller diameter (i.e., a small radius of curvature) exerts a much higher electrostatic field surrounding the wire; correspondingly much higher electrostatic stresses (i.e., Maxwell stresses) are induced to initiate droplet jetting. Furthermore, destabilization of a droplet on a small-diameter wire results in a deformed droplet with typically a smaller radius of curvature, which also leads to higher electrostatic surface traction onto the droplet to initiate droplet jetting.[45]

Figure 6 shows the FE-SEM micrographs of the PAN nanofibers collected in the present test at four different PAN concentrations. It can be observed that the nanofiber diameter increases rapidly with increasing PAN mass concentration of the PAN/DMF solutions from ~200 nm at 4 wt. % up to ~8 μm at 16 wt. %. In addition, as shown in Fig. 7, the fiber diameter deviation becomes

TABLE I. Surface tension of PAN/DMF solutions at varying PAN mass concentration.

PAN mass concentration (%)	Surface tension (mN/m)
Pure DMF	37.13 ± 0.04
0.05	36.73 ± 0.11
0.5	36.54 ± 0.09
1	36.72 ± 0.16
2	36.37 ± 0.18
4	36.65 ± 0.17
8	36.63 ± 0.05
12	36.49 ± 0.22

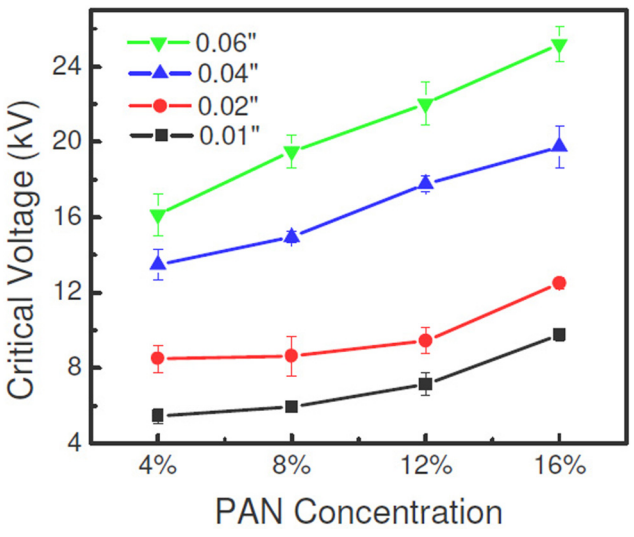

FIG. 5. Variation of the threshold electrical voltage with varying PAN mass concentration of PAN/DMF solutions with four wire diameters of 0.254, 0.508, 1.016, and 1.524 mm (i.e., 0.01, 0.02, 0.04, and 0.06 in.), respectively. Wire-to-collector distance: 165.1 mm.

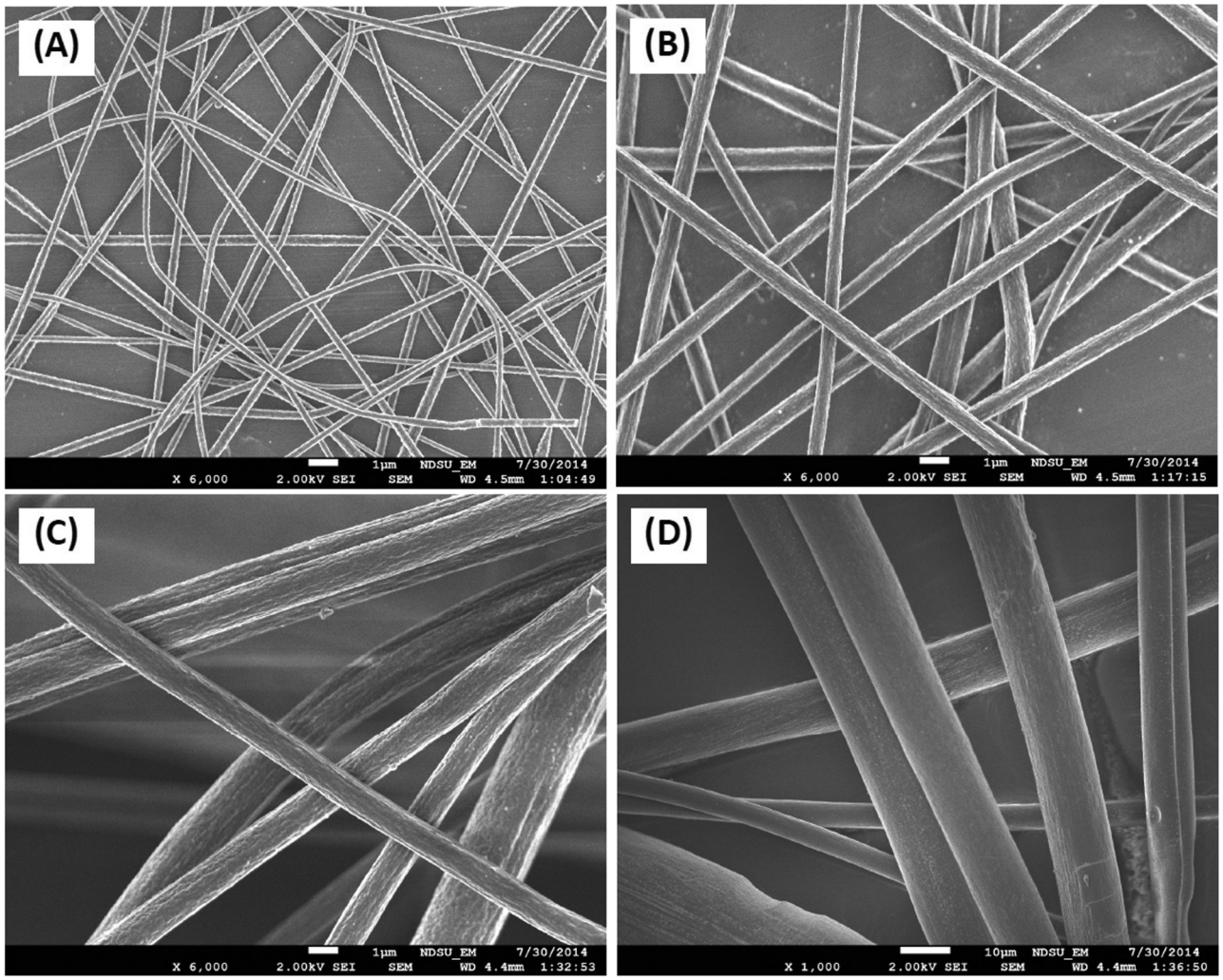

FIG. 6. FE-SEM micrographs of typical needleless electrospun PAN nanofibers prepared from PAN/DMF solutions with PAN mass concentrations: (a) 4%, (b) 8%, (c) 12%, and (d) 16%, respectively. Wire-to-collector distance: 165.1 mm.

more and more significant with increasing PAN mass concentration. Therefore, from the point of view of controllable nanofiber fabrication, a dilute polymer solution positively correlates to nanofibers of more uniform diameters in wire-based needleless electrospinning. Furthermore, experimental observations also show that the nanofiber diameter is nearly independent of the diameter of the wire electrode. In conventional needle-based electrospinning, the theoretical study has indicated that the diameter of electrospun nanofibers is independent of the initial jet diameter (i.e., the needle size).[46] In the present wire-based needleless electrospinning, the droplet size was much larger than the diameter of needles used in needle-based electrospinning. Therefore, once droplet jetting initiates, no significant difference exists between the jet formed in wire-based needleless electrospinning and that formed in needle-based electrospinning, i.e., theories that are held for determining the final nanofiber properties (e.g., the final fiber diameter) in needle-based electrospinning are also held for nanofibers produced in wire-based needleless electrospinning. In analogy, the diameter of nanofibers produced in wire-based needleless electrospinning is independent of the diameter of the wire electrode.

In addition, aqueous PEO solutions with five different PEO mass concentrations of 1%, 2%, 4%, 6%, and 8% were further employed in the present wire-based needleless electrospinning test. Figure 8 shows the similar dependencies of the threshold DC voltage to initiate droplet jetting upon the PEO mass concentration and diameter of the wire electrode. The above results indicate that a general experimental scaling law for wire-based needleless electrospinning holds for different polymer solution systems and, therefore, can be used as a strategy for controllable mass production of continuous nanofibers.

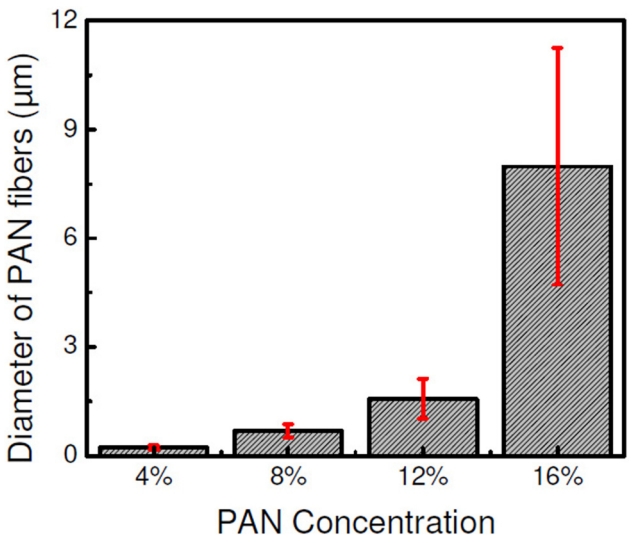

FIG. 7. Variation of the diameter distribution of electrospun PAN fibers with the PAN mass concentration in PAN/DMF solutions. Wire-to-collector distance: 165.1 mm.

C. Phenomenological model of the electrostatic force between conductive wire and fiber collector

In wire-based needleless electrospinning, it is rather challenging to determine the exact electrostatic force to destabilize the droplet to trigger jetting as such electrostatic force is closely related to the unknown varying geometrical configuration of the droplet assumed on the thin wire in the electrostatic field. Hereafter, the effects of the droplet configuration and electrocapillary deformation are ignored for a simplified approach to estimate the electrostatic force acting on the droplet. A simple electrostatic model can be formulated to explore the rational understanding of the electrostatic force acting on the wire and droplet. As the first approach, effects of the droplet and device edges are ignored and the wire-based needleless electrospinning setup is, therefore, simply modeled as an electrostatic capacitor made of two infinitely long circular cylinders with the radii of R_1 and R_2, respectively, and the spacing between two central lines d ($d = R_1 + R_2 + \Delta$, Δ is the gap between the two cylinder surfaces), as shown in Fig. 9 ($R_2 \to \infty$ for a flat-plate nanofiber collector). In this case, the capacitance per unit length of the two cylinders is[45,47]

$$C = \frac{2\pi\varepsilon}{\cosh^{-1}\left(\frac{d^2 - R_1^2 - R_2^2}{2R_1R_1}\right)} (\mathrm{F/m}), \tag{2}$$

where ε is the absolute dielectric permittivity (F/m). By assuming that a DC voltage V (Voltage) is applied between the wire electrode and the nanofiber collector (i.e., two circular cylinders), the electrostatic energy stored in the two cylinders per unit length is

$$U = \frac{1}{2}CV^2 = \frac{\pi\varepsilon V^2}{\cosh^{-1}\left(\frac{d^2 - R_1^2 - R_2^2}{2R_1R_1}\right)} (\mathrm{J/m}). \tag{3}$$

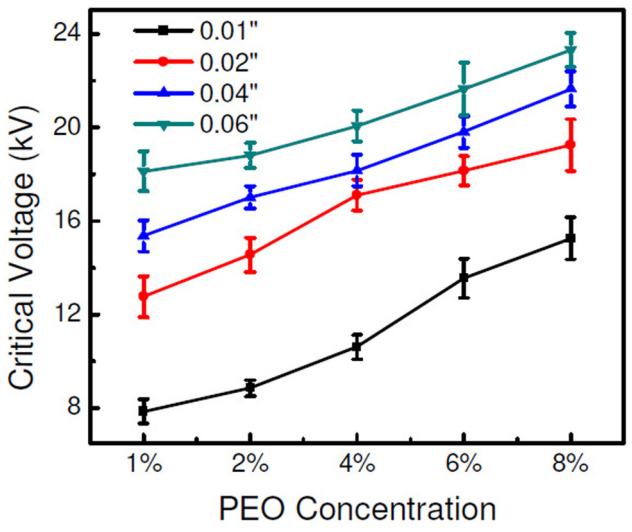

FIG. 8. Variation of the threshold electrical voltage with varying PEO mass concentration of aqueous PEO solutions for four different wire diameters of 0.254, 0.508, 1.016, and 1.524 mm (i.e., 0.01, 0.02, 0.04, and 0.06 in.), respectively. Wire-to-collector distance: 165.1 mm.

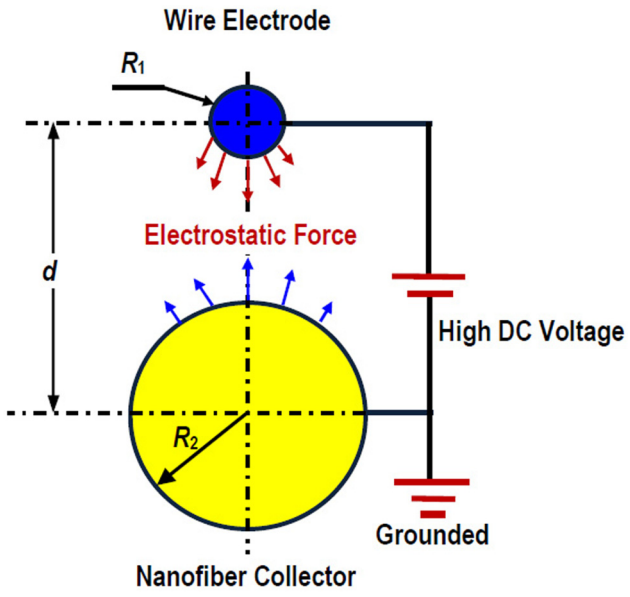

FIG. 9. Electrostatic model of a wire-based needleless electrospinning setup (cross section) ($R_2 \to \infty$ for a flat-plate fiber collector used in test).

Therefore, the electrostatic force F (N/m) between the two cylinders per unit length (m) can be determined as

$$F = \frac{\partial U}{\partial d} = \frac{\pi\varepsilon V^2}{\left[\cosh^{-1}\left(\frac{d^2 - R_1^2 - R_2^2}{2R_1R_2}\right)\right]^2} \frac{1}{\sqrt{\left(\frac{d^2 - R_1^2 - R_2^2}{2R_1R_2}\right)^2 - 1}} \frac{d}{R_1R_2} (\text{N/m}). \quad (4)$$

In the case of a flat-plate nanofiber collector, $R_2 \to \infty$ and $d = R_1 + R_2 + \Delta$. The electrostatic force between the wire electrode and the nanofiber collector per unit length is

$$F|_{R_2\to\infty} = \lim_{\substack{R_2\to\infty \\ d=R_1+R_2+\Delta}} \frac{\pi\varepsilon V^2}{\left[\cosh^{-1}\left(\frac{d^2 - R_1^2 - R_2^2}{2R_1R_2}\right)\right]^2} \frac{1}{\sqrt{\left(\frac{d^2 - R_1^2 - R_2^2}{2R_1R_2}\right)^2 - 1}} \frac{d}{R_1R_2} = \frac{\pi\varepsilon V^2}{\ln^2\left[1 + \Delta/R_1 + \sqrt{\Delta^2 + 2\Delta R_1}/R_1\right]} \frac{1}{\sqrt{\Delta^2 + 2\Delta R_1}} (\text{N/m}). \quad (5)$$

In a practical wire-based needleless electrospinning setup, the gap (spacing) Δ between the wire electrode and the nanofiber collector is much larger than the radius of the wire electrode, i.e., $\Delta \gg R_1$. In this case, the driving force F acting on the wire can be further reduced as

$$F_{R_2\to\infty,\ \Delta/R_1\to\infty} = \frac{\pi\varepsilon V^2}{\ln^2(1 + 2\Delta/R_1)} \frac{1}{\Delta} (\text{N/m}). \quad (6)$$

Relation (6) indicates that at a fixed gap (spacing) Δ, the driving force F (N/m) acting on the wire electrode per unit length decreases with decreasing wire diameter. However, from relation (6), the average body force f acting on a unit volume of a thin layer (with thickness t) of a polymer solution wetting on the wire electrode is

$$f = \frac{F_{R_2\to\infty,\ \Delta/R_1\to\infty}}{2\pi R_1 t} = \frac{\varepsilon V^2}{2\Delta t \ln^2(1 + 2\Delta/R_1)} \frac{1}{R_1} (\text{N/m}^3). \quad (7)$$

It can be validated that in the present case of $\Delta \gg R_1$, $df/dR_1 < 0$, i.e., the average electrostatic body force acting on the polymer layer on the wire electrode increases with decreasing wire radius R_1. Thus, relation (7) can be used to phenomenologically explain that under the same voltage, a wire electrode of smaller diameter leads to a larger electrostatic body force on the polymer solution, i.e., a small-diameter wire electrode corresponds to a low threshold voltage to evoke droplet jetting. Nevertheless, more accurate analysis of the electrostatic force acting on the droplet requires determining electrocapillary deformation of the droplet on the wire electrode, which is challenging due to the complicated droplet morphology to assume and needs to seek purely computational electrostatics involving electrocapillary deformations.

IV. CONCLUSIONS

Wire-based needleless electrospinning is capable of realizing low-cost, continuous, scalable nanofiber fabrication with well controlled fiber diameter. In this study, a detailed experimental investigation has been performed to examine the effects of two important material and process parameters, i.e., polymer concentration and diameter of the wire electrode, on the threshold DC voltage to trigger droplet jetting. A general experimental scaling law has been obtained such that the threshold DC voltage between the wire electrode and the fiber collector to initiate droplet jetting increases with increasing polymer concentration or wire diameter. Such a scaling law has been verified in two polymer solution systems, i.e., PAN/DMF and aqueous PEO solutions, in the present study. The experimental scaling law extracted from the present study is helpful to develop an effective control strategy for low-cost mass fabrication of continuous nanofibers with well controlled fiber diameters.

ACKNOWLEDGMENTS

This work was supported partially by the National Science Foundation (Award No. CMMI-1234297) and the NDSU Development Foundation (Award Nos. FAR0021589 and FAR0031220).

REFERENCES

[1]D. H. Reneker and I. Chun, Nanotechnology **7**, 216 (1996).
[2]R. H. Reneker, A. L. Yarin, E. Zussman, and H. Xu, Adv. Appl. Mech. **41**, 43 (2007).
[3]D. H. Reneker and A. L. Yarin, Polymer **49**, 2387 (2008).
[4]Y. Dzenis, Science **304**, 1917 (2004).
[5]D. Li and Y. N. Xia, Adv. Mater. **16**, 1151 (2004).
[6]D. Lukas, A. Sarkar, L. Martinova, K. Vodsed'alkova, D. Lubasova, J. Chaloupek, P. Pokorny, P. Mikes, J. Chvojka, and M. Komarek, Text. Prog. **41**, 59 (2009).
[7]Z. M. Huang, Y. Z. Zhang, M. Kotaki, and S. Ramakrishna, Compos. Sci. Technol. **63**, 2223 (2003).
[8]C. Burger, B. S. Hsiao, and B. Chu, Annu. Rev. Mater. Res. **36**, 333 (2006).
[9]R. S. Barhate and S. Ramakrishna, J. Membr. Sci. **296**, 1 (2007).
[10]V. Thavasi, G. Singh, and S. Ramakrishna, Energy Environ. Sci. **1**, 205 (2008).
[11]X. F. Wu and Y. A. Yarin, J. Appl. Polym. Sci. **130**, 2225 (2013).
[12]X. F. Wu, A. Rahman, Z. Zhou, D. D. Pelot, S. Sinha-Ray, B. Chen, S. Payne, and A. L. Yarin, J. Appl. Polym. Sci. **129**, 1383 (2013).
[13]B. Zhang, F. Kang, J. M. Tarascon, and J. K. Kim, Prog. Mater. Sci. **76**, 319 (2016).
[14]G. Taylor, Proc. R. Soc. Lond. A **313**, 453 (1969).
[15]A. L. Yarin, S. Koombhongse, and D. H. Reneker, J. Appl. Phys. **90**, 4836 (2001).
[16]D. H. Reneker, A. L. Yarin, H. Fong, and S. Koombhongse, J. Appl. Phys. **87**, 4531 (2000).

[17]A. L. Yarin, S. Koombhongse, and D. H. Reneker, J. Appl. Phys. **89**, 3018 (2001).
[18]M. M. Hohman, M. Shin, G. Rutledge, and M. P. Brenner, Phys. Fluids **13**, 2201 (2001).
[19]M. M. Hohman, M. Shin, G. Rutledge, and M. P. Brenner, Phys. Fluids **13**, 2221 (2001).
[20]S. Tripatanasuwan, Z. Zhong, and D. H. Reneker, Polymer **48**, 5742 (2007).
[21]C. J. Thompson, G. G. Chase, A. L. Yarin, and D. H. Reneker, Polymer **48**, 6913 (2007).
[22]X. F. Wu, Y. Salkovskiy, and Y. A. Dzenis, Appl. Phys. Lett. **98**, 223108 (2011).
[23]A. L. Yarin and E. Zussman, Polymer **45**, 2977 (2004).
[24]X. F. Wu and Y. A. Dzenis, J. Phys. D Appl. Phys. **38**, 2848 (2005).
[25]D. Lukas, A. Sarkar, and P. Pokorny, J. Appl. Phys. **103**, 084309 (2008).
[26]T. Miloh, B. Spivak, and A. L. Yarin, J. Appl. Phys. **106**, 114910 (2009).
[27]O. O. Dosunmu, G. G. Chase, W. Kataphinan, and D. H. Reneker, Nanotechnology **17**, 1123 (2006).
[28]Z. P. Zhou, X. F. Wu, Y. C. Ding, M. Yu, Y. H. Zhao, L. Jiang, C. L. Xuan, and C. W. Sun, J. Appl. Polym. Sci. **131**, 40896 (2014).
[29]J. Holopainen, T. Penttinen, E. Santala, and M. Ritala, Nanotechnology **26**, 025301 (2015).
[30]B. J. Carroll, J. Colloid Interface Sci. **57**, 488 (1976).
[31]G. McHale and M. I. Newton, Colloids Surf. A **206**, 79 (2002).
[32]X. F. Wu and Y. A. Dzenis, Acta Mech. **185**, 215 (2006).
[33]A. Bedarkar and X. F. Wu, J. App. Phys. **106**, 113527 (2009).
[34]X. F. Wu, A. Bedarkar, and I. S. Akhatov, J. Appl. Phys. **108**, 083518 (2010).
[35]X. F. Wu, M. Yu, Z. Zhou, A. Bedarkar, and Y. Zhao, Appl. Surf. Sci. **294**, 49 (2014).
[36]G. McHale, M. I. Newton, and B. J. Carroll, Oil Gas Sci. Technol. **56**, 47 (2001).
[37]X. F. Wu, A. Bedarkar, and K. A. Vaynberg, J. Colloid Interface Sci. **341**, 326 (2010).
[38]A. Bedarkar, X. F. Wu, and A. Vaynberg, Appl. Surf. Sci. **256**, 7260 (2010).
[39]C. Duprat, S. Protière, A. Y. Beebe, and H. A. Stone, Nature **482**, 510 (2012).
[40]A. Suret, F. Boulogne, D. Cébron, E. Dressaire, and H. A. Stone, Soft Matter **11**, 4034 (2015).
[41]A. Suret, F. Boulogne, K. Somszor, E. Dressaire, and H. A. Stone, Soft Matter **13**, 134 (2017).
[42]R. B. Bird, R. C. Armstrong, and O. Hassager, *Dynamics of Polymeric Liquids Vol. 1 Fluid Dynamics*, 2nd ed. (Wiley Inter-Science, New York, 1987).
[43]Z. Zhou, X. F. Wu, X. Gao, L. Jiang, Y. Zhao, and H. Fong, J. Phys. D Appl. Phys. **44**, 435401 (2011).
[44]H. A. Barnes and G. P. Roberts, J. Nonnewton. Fluid Mech. **44**, 113 (1992).
[45]L. D. Landau, E. M. Lifshitz, and L. P. Pitaevskii, *Electrodynamics of Continuous Media*, 2nd ed. (Bueeerworth-Heinenann, Oxford, 1984).
[46]S. V. Fridrikh, J. H. Yu, M. P. Brenner, and G. C. Rutledge, Phys. Rev. Lett. **90**, 114502 (2003).
[47]W. R. Smythe, *Static and Dynamic Electricity* (McGraw-Hill Book Company, New York, 1950).